Utilizing multichannel electrical resistivity methods to examine the dynamics of the fresh water–seawater interface in two Hawaiian groundwater systems

Natasha T. Dimova,[1,2] Peter W. Swarzenski,[1] Henrieta Dulaiova,[3] and Craig R. Glenn[3]

Received 11 August 2011; revised 17 November 2011; accepted 22 November 2011; published 7 February 2012.

[1] Multichannel electrical resistivity (ER) measurements were conducted at two contrasting coastal sites in Hawaii to obtain new information on the spatial scales and dynamics of the fresh water–seawater interface and rates of coastal groundwater exchange. At Kiholo Bay (located on the dry, Kona side of the Big Island) and at a site in Maunalua Bay (Oahu), there is an evidence for abundant submarine groundwater discharge (SGD). However, the hydrologic and geologic controls on coastal groundwater discharge are likely to be different at these two sites. While at Kiholo Bay SGD is predominantly through lava tubes, at the Maunalua Bay site exchange occurs mostly through nearshore submarine springs. In order to calculate SGD fluxes, it is important to understand the spatial and temporal scales of coastal groundwater exchange. From ER time series data, subsurface salinity distributions were calculated using site-specific formation factors. A salinity mass balance box model was then used to calculate rates of point source (i.e., spatially discreet) and total fresh water discharge. From these data, mean SGD rates were calculated for Kiholo Bay (∼9,200 m^3/d) and for the Maunalua Bay site (∼5,900 m^3/d). While such results are on the same order of magnitude to geochemical tracer-derived SGD rates, the ER SGD rates provide enhanced details of coastal groundwater exchange that can enable a more cohesive whole watershed perspective.

Citation: Dimova, N. T., P. W. Swarzenski, H. Dulaiova, and C. R. Glenn (2012), Utilizing multichannel electrical resistivity methods to examine the dynamics of the fresh water–seawater interface in two Hawaiian groundwater systems, *J. Geophys. Res.*, *117*, C02012, doi:10.1029/2011JC007509.

1. Introduction

[2] Geophysical methods, including magnetic, ground-penetrating radar (GPR), gravity, seismic, and electrical resistivity are commonly used to study near-surface processes and deep-underground features. An advantage of the electrical resistivity (ER) method relative to other geophysical methods is that resistivity values (reported in Ohm-m) of natural materials are usually in a much larger range compared to other physical quantities. Although uncertainties in the data inversion still exist, the large range of resistivity values of earth's materials is beneficial for differentiating subsurface structures with high level of confidence. Measured resistivity anomalies are due to changes in the composition of sediment and bedrock, and in the interstitial fluids. Because the resistivity of most bedrock minerals is a few orders of magnitude higher than any type of subsurface fluid, the applied current would flow mainly through pore water, thus providing information on the presence and quality of pore water (Table 1). Porosity and intrinsic permeability which determine the level of saturation of an aquifer would therefore significantly affect ER measurements. From this perspective, ER measurements are often used to evaluate the presence and quality of pore fluids and aquifer substrate-related characteristics on land and offshore mode [*Viso et al.*, 2010]. In the "land-based" static mode used in this research the ER cable is laid on the ground and discreet measurements of the resistivity of the subsurface are taken. In coastal areas tidal induced subsurface groundwater-seawater exchange will result in different subsurface fluid distribution resulting in different resistivity images [*Reilly and Goodman*, 1985; *Urish and McKenna*, 2004; *Ruppel et al.*, 2000; *Schultz and Ruppel*, 2005; *Swarzenski et al.*, 2006, 2007]. In contrast, in the continuous "marine" mode a ∼100 m long streamer with built-in transmitter and receiving electrodes is towed behind a boat while performing continuous measurements. In this case most of the injected current will flow in the water column and thus the method is useful only in shallow (<5 m) coastal waters and gives reliable information of the sub-seafloor to up to 30 m [*Soupios et al.*, 2007; *Khalil and Monterio Santos*, 2009]. However, recently developed variation of the ER approach, i.e. controlled source electromagnetic methods (CSEM), has been designed specifically to have enhanced

[1]U.S. Geological Survey, Santa Cruz, California, USA.
[2]Institute of Marine Sciences, University of California, Santa Cruz, California, USA.
[3]Department of Geology and Geophysics, University of Hawai'i at Mānoa, Honolulu, Hawaii, USA.

0148-0227/12/2011JC007509

Table 1. Resistivity Values in Different Substrates [From *Zohdy and Jackson*, 1969]

Rock or Sediment Type	Resistivity (Ohm-m)
Clay saturated with brackish to saline water	<3
Clay saturated with brackish to fresh water	5–8
Clay, silty sand, and some gravel saturated with fresh water	11–25
Sand and coral	40–400
Weathered basalt saturated with fresh water	30–60
Fresh basalt saturated with saline water	30–40
Fresh basalt saturated with fresh water	300–700

sensitivity to the seafloor when overlain by a conductive seawater layer and was successfully demonstrated in large scale seafloor mapping in variety of geological set up [*Evans and Lizarralde*, 2011, 2003; *Hoefel and Evans*, 2001; *Mulligan et al.*, 2007]. Historically, electrical resistivity measurements have been most commonly applied to assess oil-bearing capacity of reservoir rocks [*Archie*, 1942; *Waxman and Stairs*, 1968], borehole yield from sandstone aquifers [*Worthington*, 1972; *Baker and Worthington*, 1973].

[3] Electrical resistivity measurements in volcanic areas, specifically in the Hawaiian Islands, were performed for the first time by *Swartz* [1937]. Several subsequent resistivity investigations were conducted mostly in the 1970s and 1980s on Oahu [*Zohdy and Jackson*, 1969] and the Big Island of Hawaii [*Zohdy*, 1968; *Zohdy and Jackson*, 1969]. The ER techniques used at that time were laborious and time-consuming as the receiver was a single channel unit and the electrodes needed to be moved manually after each measurement in order to obtain greater depths.

[4] Geologic, hydrologic, and climatic conditions on Hawaii yield some of the most productive freshwater aquifers [*Oki et al.*, 1999a]. Groundwater discharge to the nearshore expressed through submarine springs has been mapped and officially reported in most of the Hawaiian Islands [*Swartz*, 1937; *Stearns*, 1940]. However, the variety of hydrologic and geologic settings of the islands determines site-specific controls and mechanisms of groundwater discharge at each individual site. Our study was focused on two contrasting areas, on the Kona coast of the Big Island of Hawaii and on the southern shore of Oahu. Hydrological models have predicted brackish and fresh water groundwater discharge in these areas [*Oki et al.*, 1999b]. These predictions were confirmed recently by a series of radon (^{222}Rn) and radium (^{224,223,226}Ra) tracer studies on the west side of the Big Island reporting abundant fresh and brackish water discharge and associated nutrient fluxes [*Street et al.*, 2008; *Johnson et al.*, 2008; *Peterson et al.*, 2009; *Knee et al.*, 2010]. Along the same coastline aerial thermal infrared (TIR) images by *Johnson et al.* [2008] confirmed a large number of groundwater point-sources, and because the outcrops were so distinct these authors hypothesized that it is very likely that local geological subsurface formations such as lava tubes serve as natural groundwater conduits. These assumptions were, however, not confirmed by actual subsurface observations, although there is anecdotal evidence of submarine springs discharging from lava tubes. On the south shore of Oahu, *McGowan* [2004], *Swarzenski et al.* [2009], and *Holleman* [2011] found significant SGD, including sites at Wailupe Beach Park, Maunalua Bay (Figure 1), as fresh to brackish coastal groundwater springs. Freshwater discharge in the coastal areas of Oahu has been known for centuries and some of these vents are present even today [*Shade and Nichols*, 1996].

[5] Although there is already ample information about the magnitude of SGD at some sites in the Hawaiian Islands, our knowledge on the actual pathways and extent of movement of the fresh water–seawater interface within the coastal aquifer is very limited. The objective of this work was to utilize a multichannel, multielectrode resistivity system to examine the dynamics of the terrestrial and marine controls on the fresh water–seawater interface in coastal aquifers with contrasting geologic settings and to further develop this tool to estimate rates of SGD. While the Kona coast of the Big Island of Hawaii represents a young volcanic substrate with lava tubes and sheet joints as effective groundwater conduits, the aquifers on the south shore of Oahu are impeded by interstratified alluvium classified as a "caprock" which acts as a semi-confining layer [*Langenheim and Clague*, 1987; *Gingerich and Voss*, 2005]. However, although geologically very different, both sites exhibit groundwater discharge in the form of coastal springs as well as diffuse seepage. As presented next, this study sheds light on the short-term tidal dynamics of the fresh water–seawater interfaces with the unique opportunity to analyze the geometry of well defined groundwater conduits via ER time series measurements. In addition, we also present a novel application of these consecutive resistivity measurements to derive actual groundwater discharge rates, a method which has been developed during this study. We further describe how the same model applied in reverse can be used to evaluate seawater intrusion.

[6] The advantage of the ER approach is that it provides the dimensions and pattern of groundwater discharge, demonstrating the extent of SGD, which none of the other conventional methods, such as geochemical tracers [*Charette et al.*, 2008], aerial thermal infrared [*Johnson et al.*, 2008], seepage meters [*Taniguchi et al.*, 2003], or hydrological models [*Michael et al.*, 2005] can address. Furthermore, large scale groundwater discharge estimates based on these methods can have relatively high uncertainties and often over- or underestimate groundwater discharge due to large-scale spatial extrapolation that need to be made. Here we demonstrate that the multichannel, multielectrode resistivity system is not only useful to define the groundwater–seawater boundaries within the coastal aquifer but also to infer the geometry of groundwater conduits, the dimensions of the seepage face, and finally to derive groundwater discharge rates.

2. Study Sites

[7] The data presented here were collected at Kiholo Bay, situated on the west side of the Big Island of Hawaii, and at Wailupe Beach Park, Maunalua Bay, along the southeast coast of Oahu (Figure 1). Both islands are known to have extremely productive volcanic-rock aquifers from which groundwater discharges directly to the sea. The Big Island area has high water table levels (>12 m above sea level on

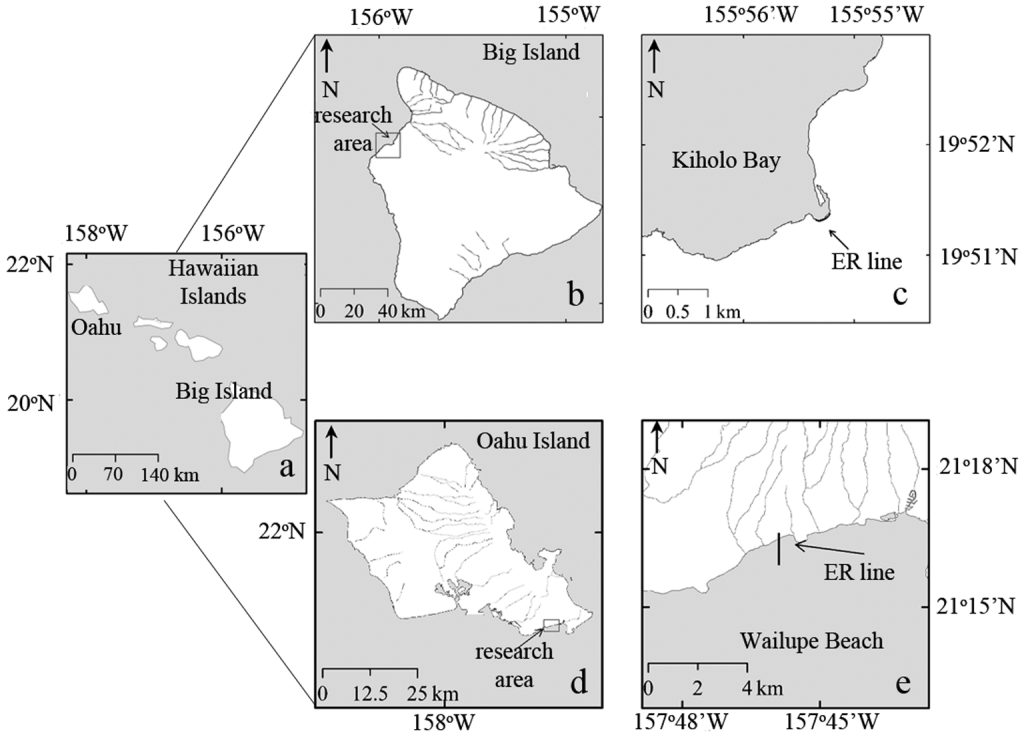

Figure 1. Maps of the location of the research areas and the position of the electrical resistivity (ER) lines: shoreline-parallel line at Kiholo Bay, Big Island and shoreline-perpendicular at Wailupe Beach, Oahu. Lengths of ER lines not to scale.

land near the shore) which are possibly associated with a buried rift zone of the Hualalai Volcano or scarps draped with lava flows. The void spaces in the sequence of lava flows creates high intrinsic permeability conditions parallel to the flows in this area [*Mullineaux et al.*, 1987]. The beach where the ER time series measurements were carried out has a relatively gentle slope and it is composed of unconsolidated black sand and pebbles. During our field work freshwater seepage at the beach face was evident regardless of tidal stage. Water table levels in the coralline limestone aquifer in southern Oahu range between 7.5 and 9 m above sea level inland and between 4.5 to 6 m above sea level near the shore where the water is under artesian pressure because it is confined by caprock [*Oki et al.*, 1999b; *Gingerich and Voss*, 2005]. The caprock impedes the fresh groundwater discharge toward the ocean (Figure 2). In the eastern part of the island, where the research area is, thick valley fill and underlying weathered rocks form partial barriers for groundwater flow. When groundwater intercepts the caprock it discharges as artesian submarine springs mostly near the inland margin of the caprock. Several nearshore small scale submarine springs (surface vents with diameter < 1–2 m) were indeed observed during our ER shoreline-perpendicular survey. The magnitude of the discharge of these springs was clearly related to the tide cycle. During the collection of ER time series continuous measurements of salinity performed

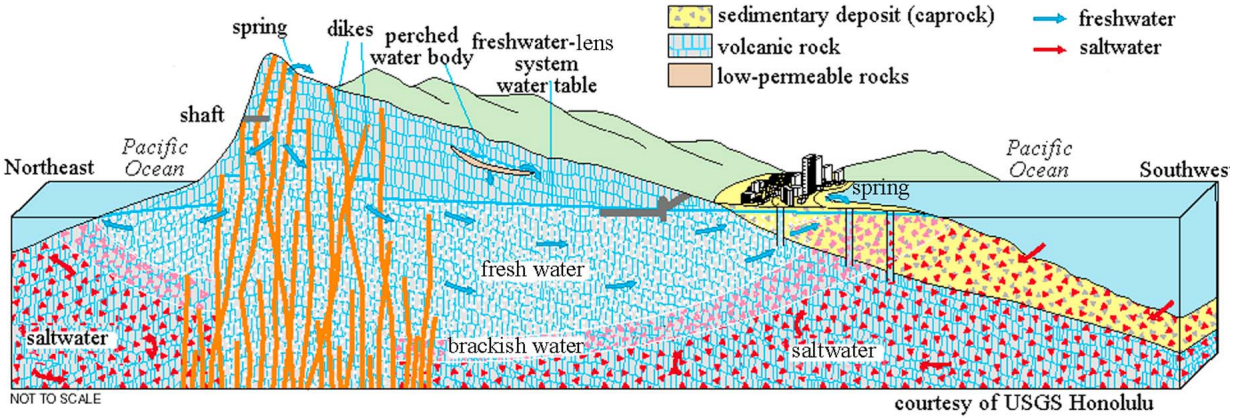

Figure 2. Hydrogelogical setting of Oahu [from *Macdonald et al.*, 1983].

by two CTD divers (Van Essen Instruments) attached to the resistivity cable indicated lower salinities at low tide compared to high tide. We also noticed that the size of the boils that appear on the seawater surface just on top of two of the springs were noticeably increasing as the low tide was progressing (Figure 5, photo). With ebbing tides the hydraulic pressure on the submarine spring decreases and groundwater discharge increases. The resistivity cable was positioned on top of these vents so that an image of the subsurface structure of their conduits vents could be obtained in addition to the observations of the fresh water–saltwater interface oscillations.

3. Methods

3.1. Archie's Law

[8] Electrical resistivity is one of the best suited geophysical tools to examine the scales and dynamics of the fresh water–seawater interface in coastal aquifers because it directly measures changes in the composition of the subsurface pore fluids. In order to evaluate fresh SGD we first calculate salinity values using resistivity and site-specific formation factors inferred from time series ER measurements and data for resistivity of collected pore water from piezometers probing the subsurface at the place where the ER measurements were acquired. The formation factor (F) is a specific characteristic of the mineral composition of an aquifer, its porosity, and composition of the saturated fluids. The relationship between formation factor and porosity (φ) is given by Archie's law [*Archie*, 1942]:

$$F = a \times \varphi^{-m} \tag{1}$$

where φ is the porosity of the media (%), F is the formation factor of the subsurface (dimensionless), and the two coefficients "a" and "m," also known as Archie's coefficients, reflect the physical properties of the aquifer [*Winsauer et al.*, 1952; *Keller and Frischknecht*, 1966; *Jackson et al.*, 2002]. Archie's coefficients often vary over a large range and are difficult to evaluate due to natural heterogeneity of the subsurface [*Jackson et al.*, 2002; *Worthington*, 1993]. However, for fully saturated substrate Archie's law can be expressed also as:

$$F = \frac{R_f}{R_p} \tag{2}$$

where R_f in the resistivity of the porous medium measure by ER instrumentation [Ohm-m] also referred to as formation resistivity, and R_p is the resistivity (Ohm-m) of the pore fluid. For the purpose of our calculations we used formation factor values obtained from equation (2) and ER data of the porous medium (R_f) to calculate the resistivity of the pore fluid (R_p) for each individual data point of our ER time series. The relationship of salinity (S) and conductivity/resistivity is well-established [*Perkin and Lewis*, 1980; *Fofonoff and Millard*, 1983]. In our calculations we use a formula proposed by *Manheim et al.* [2004]:

$$S = 7.042 \times R_p^{-1.0233} \tag{3}$$

3.2. ER Data Acquisition

[9] Resistivity readings of the substrate are acquired by injecting direct current into the ground through two current-producing electrodes, C_1 and C_2, and measuring the resulting voltage difference (ΔV) in two potential electrode pairs; P_1 and P_2 (V) (Figure 4a). The apparent resistivity (ρ_a), i.e., resistivity values (Ohm-m) collected of an ideally homogeneous subsurface that are independent of electrode configuration, is then calculated using equations (4) and (5):

$$\rho_a = K \times \frac{\Delta V}{I} \tag{4}$$

and

$$K = \frac{1}{2\pi}\left[\frac{1}{\left(\frac{1}{r_1}-\frac{1}{r_2}\right)-\left(\frac{1}{r_3}-\frac{1}{r_4}\right)}\right] \tag{5}$$

where I (A) is the injected current, K (m) is called geometric factor, and r_i (m) is the electrode spacing [*Loke*, 2011]. Since the apparent resistivity is proportional to the geometric factor K (respectively r_i), one could obtain deeper ER profiles by increasing the distance between the current and the potential electrodes (equation (5)). However, because the total resistance in the electrical path increases as electrode spacing is increased, to be able to record the effects of the current flow through a potential difference which decreases in size, a more powerful current source is required. There are several different electrode configurations, so-called arrays that can be used to collect resistivity data including Wenner, Schlumberger, pole-pole, pole-dipole, and dipole-dipole. In a dipole-dipole configuration, such as the one we have used in this study, the current electrodes C_1 and C_2 and potential electrodes P_1 and P_2 are grouped in close pairs that form a current and a potential dipole (Figure 3b). Some of the advantages of the dipole-dipole array over Wenner or Schlumberger arrays include (1) higher sensitivity to horizontal changes which allow for bilateral investigations, (2) minimum current leakage, and (3) minimized problems with inductive coupling [*Zohdy*, 1968; *Zohdy et al.*, 1974; *Loke*, 2011]. Among the disadvantages of the dipole-dipole methods are requirements for a large current source, a high sensitivity resistivity meter that can register small changes in resistivity, and solid ground contact of the electrodes. Field data and modeling experience show that reliable data (low uncertainty values) can be collected in a dipole-dipole electrode configuration up to depths that are typically 20–30% of the length of the cable array depending of the composition of the porous medium subsurface [*Loke*, 2011]. Using a dipole-dipole electrode configuration in a manual mode, *Zohdy and Jackson* [1969] reported resistivity values between 3 and 700 Ohm-m for Oahu and the Big Island of Hawaii, for various substrate types and degrees of saturation.

[10] The data presented here were collected with a Super Sting R8/IP unit, an 8-channel receiver (Advanced Geosciences Inc., AGI), connected to 112 m streamer (56 electrodes, spaced 2 m apart) via an external switching box (Figure 3d). With this instrumentation, deeper electrical signal penetration is achieved by switching the dipole pairs "on" and "off" along the streamer line (Figure 3c). Stainless steel stakes (~40 cm long) were usually used to assure solid

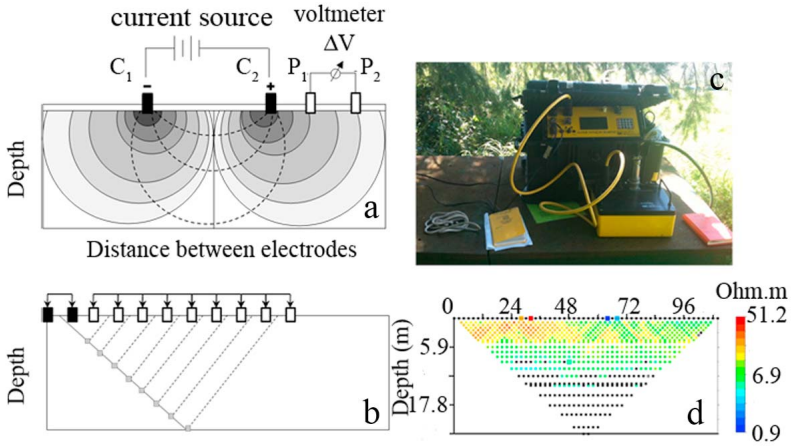

Figure 3. (a) Schematic diagram showing principle of DC (direct current) resistivity data collection in a dipole-dipole configuration; dashed line indicates the current flow; circles in different gray color present the equipotential voltage lines (modified from *Loke* [2011]). (b) Schematic represents the principle of data collection used by 8-channel Super Sting R8/IP instrumentation. (c) The front panel of the instrument and the switching box. (d) An example of a scatterplot of surface apparent resistivity data: the red and orange squares on the resistivity line are the two current electrodes (C_1 and C_2), and the blue light and dark are the receiving, potential electrodes (P_1 and P_2). Noisy data are shown as black dots; these values were eliminated in the inversion process.

ground contact. Particularly in unsaturated portions of the cable, the contact resistance was decreased by keeping the electrodes and substrate moist by frequent watering. Measurements were collected using a dipole-dipole electrode array powered by a single 12 V deep-cycle marine battery. The user-defined maximum current applied for each measurement was 1,250 mA and the receiver was set up to take measurements every 1.2 s with a maximum acceptable error set at <3%. With a 56-electrode cable collecting measurements of streamer arranged in dipole-dipole configuration, it took 26 min to complete a full data set of 762 measurements.

3.3. Data Inversion of ER Measurements

[11] To determine the true subsurface resistivity, an inversion process of the measured data, presented as apparent resistivity must be used [*Loke*, 2011; *Samouelian et al.*, 2005]. For this work, we used Earth Imager 2D (AGI software) to perform the inversion. The main goal of the inversion is to define a model that can predict true resistivity values under the same electrode configuration as the one used in the real measurements and based on a prediction of the resistivity distribution per initial model parameters. The output of this model is a reconstruction of the true resistivity subsurface distribution under certain restrictions that are defined in the initial model parameters and the model. The model is a partial differential equation that governs the relationship between data and model parameters. A non-unique solution of this equation is obtained per a set of predefined conditions, or model parameters. The Earth Imager 2D software offers several user-defined inversion models. For our inversions we used the Smooth Model, also known as Occam's inversion, which is recommended as a stable and robust approach regardless of the signal-to-nose ratio of the data [*Constable et al.*, 1987]. Occam's inversion finds the smoothest possible model whose response fits the data to an a-priori Chi-square statistic avoiding introducing unnecessary structure into the model. The Smooth Model is based on the assumption of Gaussian distribution of data errors. More detailed information about the other methods is given by *Ernstson and Kirsh* [2006].

3.4. Statistical Evaluations of ER Subsurface Distributions

[12] Multiple iterations of the model are run until certain criteria for best fit between the predicted and measured resistivity values are met. Two parameters are used in Earth Imager 2D to evaluate how good the fit is: the root mean square error (RMS) in percentage and the L2-norm [*Advanced Geosciences, Inc.*, 2009]. The main reason for high RMS is usually noisy raw data. It is common practice to inspect the raw resistivity data for noise and either manually or using user-defined software criteria to remove data points. Often noisy data are caused by poor electrode ground contact, which results in low signal strength (low signal-to-noise ratio). The depth of penetration at dipole-dipole geometry is relatively shallower compared to the other configurations and thus the depth of sensitivity (which ultimately depends on the structure of the subsurface) when using this electrode configuration is expected to be lower (Figure 3c).

[13] The L2-norm is defined as the sum of the squared weighted data errors:

$$L2-norm=\sum_{1=1}^{N}\left(\frac{\left(d_i^{calc}-d_i^{meas}\right)}{w_i}\right)^2 \qquad (6)$$

where N is the number of measurements; W_i is the data weight, d_i^{calc} is the calculated data, d_i^{meas} is the measured

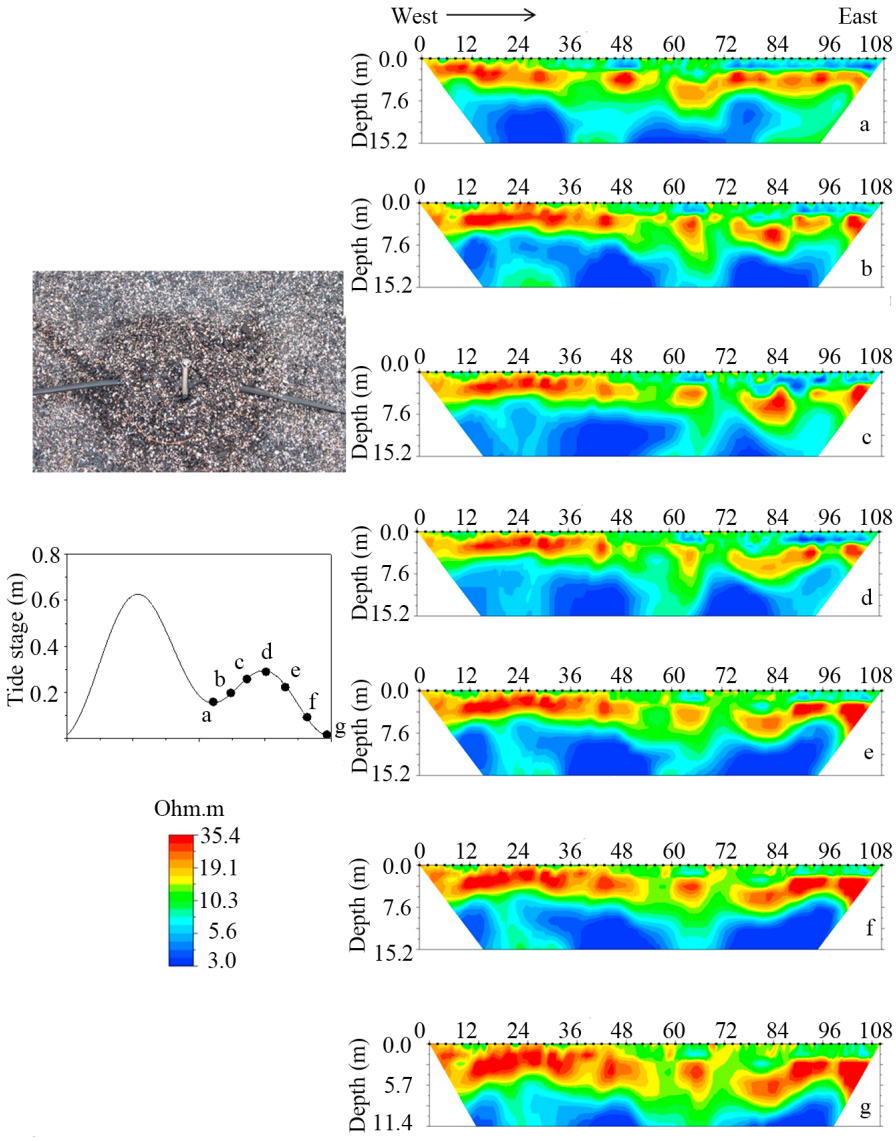

Figure 4. Shoreline-parallel seven-step time series carried out at Kiholo Bay, Big Island (Figure 1c) during 12-h tide cycle. The contact surface is coarse "black sand" shown on the picture on the top left panel. The letters from the tide plot correspond with the letters on the images on the right panel. Statistical evaluations of the inversion model in terms of RMS error and L2-norm are presented underneath each image; numbers on top indicate the length of the ER cable (m).

data. Because the number of measurements could be different, the normalized L2-norm is usually used:

$$normalized\,L2-norm=\frac{L2-norm}{N} \tag{7}$$

when the normalized L2-norm reaches 1.0 or smaller, the inversion is converged. Good fit is generally considered to be when the RMS error is below 10% and the L2-norm value is less than 5%.

3.5. Evaluating Fresh Water Discharge Using ER Time Series Measurements and Salinity Box Model

[14] To evaluate fresh SGD in this study we developed a new approach that relies on the subsurface fresh water source distribution obtained from ER images and salinity evaluations based on calculated site-specific formation factors ground-truthed by pore water piezometer data for high and low tide conditions as previously described in section 3. Fresh water seepage rates were derived using a salinity mixing model presented by *Dimova et al.* [2011] and modified to reflect these specific scenarios. For this approach we analyzed ER images from the time series to define the boundaries of subsurface groundwater flows. To identify the exact dimensions of the areas of preferential fresh water subsurface flows we used an option of the Earth Imager 2D software that performs a difference inversion between two consecutive images taken during different hydrologic conditions in the same area (i.e., during two different tidal stages at the same position of the ER array). In this procedure the

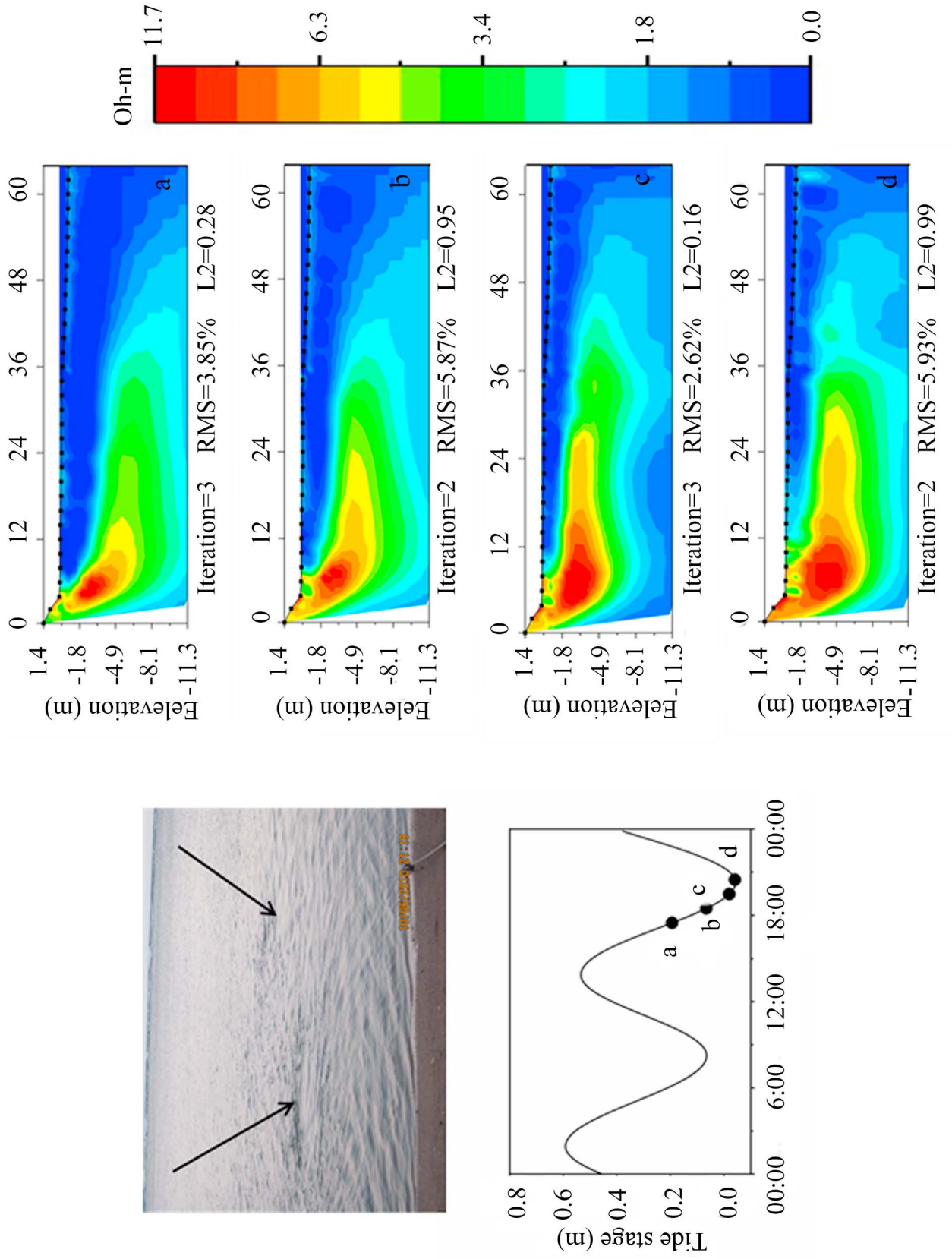
Oh-m
11.7
6.3
3.4
1.8
0.0
a
b
c
d
Elevation (m)
1.4
-1.8
-4.9
-8.1
-11.3
0
12
24
36
48
60
Iteration=3 RMS=3.85% L2=0.28
Iteration=2 RMS=5.87% L2=0.95
Iteration=3 RMS=2.62% L2=0.16
Iteration=2 RMS=5.93% L2=0.99
Tide stage (m)
0.8
0.6
0.4
0.2
0.0
00:00
6:00
12:00
18:00
00:00

Figure 5

software treats one of the data sets from the time series as the base against which the other is compared. Using the same model inversion settings, it then produces difference images between any monitoring data set and the base data set. We chose to use the ER data set acquired during high tide as our base set, as we were interested in the groundwater discharge rate per tidal cycle when there is the largest difference between tidally influenced hydraulic head. This also allows us to observe the largest shifts in the seawater-fresh water interface within the aquifer. Constraining the size of each area we then calculate average salinity within each segment during high (S_h) and low (S_l) tide. To calculate the volume (using 1 m as the third dimension) of the fresh SGD (V_{sgd}) we use mass and salt balance equation (equation (8)) where fresh water inflow derived from land balances SGD export into the ocean:

$$S_h V_{sal} = \left[V_{sal} + V_{sgd}\right] S_l \quad \text{or} \quad V_{sgd} = V_{sal} \frac{[S_h - S_l]}{S_l} S_l \qquad (8)$$

where V_{sal} is the constant volume of the defined area of change based on the base and monitoring ER images which is fully saturated with salt water during high tide; V_{sgd} is the unknown discharged or exported volume of fresh water for the time interval between high and low tide; and S_h and S_l are the average salinities in the selected box of preferential flows respectively during high and low tide. The main assumption in the model is that the entire volume of fresh water V_{sgd} is exported to the surface so that the volume of the selected box of preferential flow does not change, i.e., the principle of conservation of both mass and salt is applied. This equation also does not account for saltwater dispersion (or diffusion) during the tidal water masses exchange. We also attempted to calculate seawater intrusion using the same approach in reverse, i.e., using data collected during rising tide. In this scenario one would assume that the water table will rise proportionally to the volume of seawater replacing freshwater in the voids of the aquifer. The accumulated uncertainty of these reported seepage rates is a result of several factors including: (1) uncertainties of the ER measurements; (2) uncertainties of real data to model results misfits from the inversion; and (3) uncertainties from salinity measurements used in the procedure for calculating formation factors. The first category of uncertainty was controlled by a user-defined acceptable error in the process of collecting the ER data. For all our measurements we set up this threshold at 3%. The second source of errors is a result of the inversion process and is reported by the software as RMS and L2 misfit. In all cases both parameters never exceeded 10% and in most cases these values were below 5%. The last source of uncertainties is defined by the actual salinity measurements of pore water performed in the field. We used a handheld YSI 85 for which the manufacturer reports an error <5% for the salinity measurements. Therefore, our main source of uncertainty is a result of the inversion of the data in which case is no more than 10%.

3.6. Previous Estimates of SGD Using Tracers Approach

[15] Previous SGD study at Kiholo Bay [*Peterson et al.*, 2009] reported 6,300 m^3/d fresh water ^{222}Rn-derived-SGD rates. This evaluation was assigned to a single point source whose plume dimensions were assessed from TIR images and salinity profiles in the northern part of the bay. Preliminary results from a seepage meter study [*McGowan*, 2004] yielded a total SGD in Wailupe Beach Park of around 30,000 m^3/d, while very recent work based on ^{222}Rn estimated the total SGD (recirculated seawater and fresh water discharge) into Wailupe Bay to range between 48,200 m^3/d and 95,500 m^3/d based on a 400-m width of the beach based on a tracer distribution survey [*Holleman*, 2011], and 6,000 m^3/d at Niu Bay (east side of Mauanlua Bay) [*Swarzenski et al.*, 2009].

4. Results

4.1. Resistivity Surveys at Kiholo Bay

[16] The ER shoreline-parallel time series measurements at Kiholo Bay were carried out on September 26, 2010 for 12 h (Figure 1c). We were able to take seven "snap-shots" of the subsurface resistivity distributions during one tidal cycle (Figure 4). Resistivity values ranged between 3 and 35.4 Ohm-m with a maximum depth penetration below ground of about 12 m. During the ER survey freshened groundwater discharge was manifested by multiple different size rivulets with lower salinity. These were observed at the beach face close to the tide line both during low and high tide, with distinctive larger seepage occurring during low tide. This was especially evident at the west side of the research area that corresponds with the beginning of our ER array (Figures 4a–4g). High resistivity values (19 and 35 Ohm-m) were observed along the first 30 m of the streamer and appeared to coincide with field observations of active fresh water seeps. All seven inversions resulted in RMS errors < 7% and L2-norm < 2.5 (most cases less than 1). These results were obtained while suppressing noisy data, which in all cases was mostly deeper than 12 m. The best fit under these initial conditions was obtained in the second data set of the Kiholo Bay experiment (Figure 4b). Software statistical evaluations show that it takes five iterations with the selected settings for the model to converge at RMS error 3.84% and L2-norm 0.92. Relative percentage of data misfit pseudo-section diagrams generated by the software indicates that a small part of the data, mostly at larger depth at the east side of the profile, has a misfit of about 20%. Using the resistivity difference image produced by the Earth Imager 2D software we identified and analyzed the resistivity patterns of five separate sections (A, B, C, D, and E) that correspond to

Figure 5. Shoreline-perpendicular time series performed in Wailupe State Park, Oahu (Figure 1e) during falling tide. Arrows on the picture on the top left panel indicate the position of the two artesian submarine springs that were found during our field work. The letters from the tide plot correspond with the letters on the images on the right panel and statistical evaluations of the inversion model in terms of RMS error and L2-norm are presented underneath each image. In this case the *y* axis is presented as elevation above sea level to reflect the topography and bathymetry of the area where the ER cable was deployed.

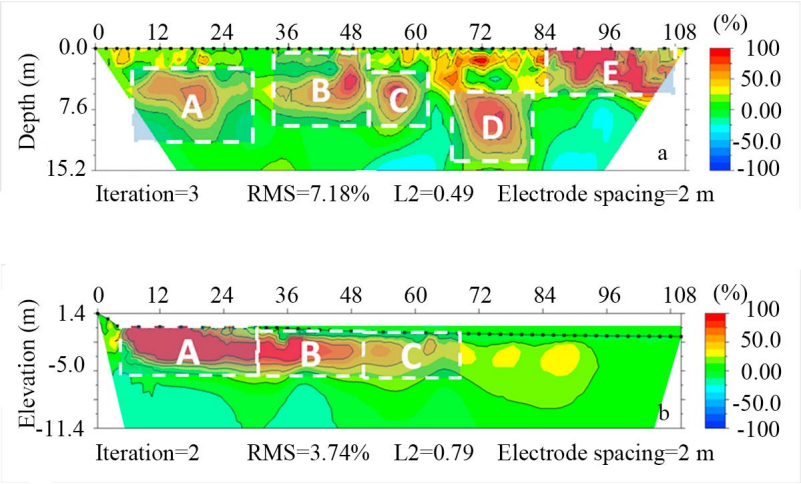

Figure 6. Percent difference change in resistivity between high tide and low tide scenarios at (a) Kiholo Bay and (b) Wailupe Beach. Areas showing preferential flows are analyzed in the salinity box model for evaluation of groundwater discharge in this area.

zones of preferential flows at the Kiholo Bay site (Figure 6a). To calculate the amount of fresh water that causes the observed ER changes in the images, we treated each of these sections containing a distinct groundwater conduit as an individual box. Resistivity measurements were converted to salinity via equation (3) for high and low tide scenarios and the volume of the discharged fresh groundwater that must be delivered to each individual box to result in the observed salinity changes is then calculated via equation (8). We assumed that this volume of water was then exported into the ocean as SGD in the time interval between high and low tide. The calculated volumes of fresh water discharge through each of the five identified conduits at the beach face of Kiholo Bay during our measurements are presented in Table 2. The total fresh water discharge, i.e., the sum of all five single sources, was estimated at ~4,600 m^3. Based on these methods and assumptions (i.e., semidiurnal tide within 24 h), the total discharge would be at least 9,200 m^3/d for a 110-m long section (equal to the span of our cable) and in the shallow aquifer (only above 12 m depth) of the Kona coastline.

4.2. Resistivity Surveys in Wailupe Beach Park, Maunalua Bay, Oahu

[17] Time series ER measurements during falling tide were carried out at Wailupe Beach Park, Maunalua Bay on October 6, 2010 (Figure 1d). The electrical cable was placed perpendicular to the shoreline following the natural slope of the beach (Figure 1e). During our measurements about two-thirds of the cable was under seawater with a larger portion submerged during high tide. An inversion of shoreline-perpendicular data sets collected during such conditions requires additional corrections that account for the topography and bathymetry of the array. Such site-specific corrections were applied to our model parameters before the inversion of the Wailupe Beach Park ER time series. Although tide observations from depth transducers (CTD divers attached to the 8th and 56th electrodes indicated that the water level did not change significantly for the duration of our measurements (~0.3 m), we found that the overlying water column had significantly affected large portions of the collected resistivity data resulting in poor signal-to-noise ratios. These data, mostly collected in the seaward portion of the cable (after 65th meter) did not pass the 3% error threshold in the inversions process and were further eliminated from our calculations and from the ER images presented in Figure 5. The initial model run in the range between 1 and 12 Ohm-m yielded statistically significant results at a depth up to 11 m. The inversion with these settings of all data resulted in RMS errors < 6%, and L2-norm <1. With this data filtering the best statistics were obtained in the inversion of case C (low tide). The RMS error in this case was below 3% and the L2-norm 0.16. Data misfits (<9%) were observed mostly on the surface seaward side of the cable and below 8 m depth. A similar approach to the one presented for Kiholo Bay was applied to evaluate fresh water discharge at Wailupe Beach Park, southeastern Oahu (Figure 1e). Several submarine springs were observed in the area during our survey. Two of them were also detected by our streamer and can be clearly

Table 2. Fresh Water Discharge Through the Different Domains in Kiholo Bay

Source	Cable Length (m)	Depth (m)	Offshore Extent (m)	Box Volume (m^3)	Calculated SGD (m^3/d)
A	18	5.7	1	103	1702
B	14	3.8	1	53	1013
C	8	5.7	1	46	666
D	12	3.8	1	46	1092
E	20	5.7	1	114	157

identified at the beginning of the array (Figures 5a–5d, between 8th and 12th meter down cable). To facilitate the resistivity/salinity calculations we grouped the area into three boxes (Figure 6b). Changes in the average salinity values based on all three boxes between high and low tide were used to calculate discharge rates during the falling tide period. For the period of our measurements we assessed total fresh SGD of about 2,950 m^3. The total fresh water discharge for a semidiurnal 24-h tide cycle would then be about 5,900 m^3/d per 65-m offshore extent of the cable.

5. Discussion

[18] The main goal of this study was to verify previous hypotheses that SGD in volcanic areas and specifically in these two study sites manifests as point sources via lava channels and as submarine springs. In order to identify these hydrogeological features and subsurface SGD dynamics we deployed arrays at fixed locations and performed time series during a tidal cycle. Such "static" approach of the technique gave us the opportunity to observe subsurface changes that are due only to changes in the pore water composition and eliminate possible effects of different geology.

[19] A seven-step time series resistivity image was produced from an array during a tidal excursion at Kiholo Bay, Big Island of Hawaii, in order to quantitatively compare images to assess where the greatest change in resistivity has occurred (i.e., where the dynamics of the freshwater-seawater interface induce the greatest water exchange). Because our ER array at Kiholo Bay was deployed parallel to the shoreline and based on information about the geology of the area [*Mullineaux et al.*, 1987; *Oki et al.*, 1999b], we hypothesize here that the images from this ER survey reveal actual cross sections of lava tubes and lava flows that convey terrestrial fresh water discharge into the ocean (Figure 4). Although the size of such volcanic structures naturally can have a wide variability, the dimensions of the subsurface features we observed (10–15 m and larger) are similar to previously observations [*Macdonald et al.*, 1983; *Mullineaux et al.*, 1987]. Confidence that these are permanent geological features is based on the fact that all these areas of enhanced resistivity were present at specific depths of the profiles in each one of the seven ER images taken during a tidal cycle. Resistivity "by difference" data inversion further confirmed that the same regions are the main areas of large resistivity changes (up to 100%) during the transition from high to low tide (Figure 6a). Because the ER cable is positioned at the same place i.e., does not move during the time series measurements, the observed changes must be due to hydrologic changes, not geologic in nature. Increasing the overall diameter and the size of the high resistivity sections from high to low tide is an additional evidence of fresh water flow increase due to changes of the hydraulic gradient at the beach face. Such behavior was clearly observed in all sections. Image results from an inversion of resistivity data are reported with certain confidence level of statistical significance as the inversion itself in general is an iteration process of matching original data with data predicted by a chosen model [*Loke*, 2011]. As mentioned earlier, statistical parameters such as RMS error, L2-norm, and misfit plots are common measures of how well the chosen model fits the real data, i.e., how realistic are the calculated resistivity values. From statistical point of view results with RMS errors less than 5% and L2-norm $\sim$1 are considered highly significant. Of all seven inversions of the Kiholo Bay data set only one was evaluated with a RMS error and L2-norm slightly above this threshold, RMS error 6.7 and L2-norm 2.8 (Figure 4c). Calculated misfit between measured and predicted resistivity values indicate that only a very small part of our data at lower depths has a misfit of <20%. The high statistical evaluations of the obtained resistivity values gives us assurance that the calculated site-specific formation factors and the salinity values based on these measurements are realistic and thus the final reported fresh SGD single-point seepage rates are reasonable. The ER-derived fresh water SGD rates in Kiholo Bay are also on the same order of magnitude with previously reported tracer-derived estimates [*Peterson et al.*, 2009]. However, in addition to these evaluations, the ER approach allowed us to locate the exact position and to identify and analyze with high level of certainty the geometry and the scale of several single sources of groundwater discharge during a full tidal scale (Figure 6a). Real-time oscillations of the fresh water–seawater interface due to changes in the hydraulic gradient during a tidal cycle were also observed.

[20] In Wailupe Beach Park, in southeastern Oahu we deployed the 56-electrode electrical cable perpendicular to the shore line (Figure 1e) as our main goal was to identify the offshore extent of groundwater discharge. Our resistivity measurements at Wailupe Beach Park demonstrated that the extent of the seepage face reaches at least 65 m offshore (Figure 5). Anecdotal evidence from local residents is that cold seeps can be felt as far as the reef's edge 500 m offshore. Indeed, because of the presence of the caprock one cannot expect the "usual" exponential decrease of SGD over distance presented by *Taniguchi et al.* [2003] and *Cable et al.* [1996], nor can this setting be compared to the scale of groundwater discharge processes on extensively studied passive shelf margins as discussed by *Bratton* [2010]. Our study clearly identified that SGD in the Wailupe region occurs both as diffuse seepage and brackish submarine springs as demonstrated in Figure 5. The four images obtained from the electrical resistivity time series carried out at Wailupe Beach Park show very clear enhanced upward groundwater flow along the streamer. The zone that was most dramatically affected by the subsurface hydrological changes during the tidal cycle coincides with the beginning of the cable, i.e., between 0 and 4th m. As the low tide progresses similar changes in the subsurface resistivity distribution are also evident farther along the line at 6th and 8th meter. Because of the shape of these images and the fact that several submarine springs were observed during in the area during the survey, we hypothesize these are probably images of "vent"-type geohydrological features. The diffuse seepage is apparent from the images as a less intense higher resistivity layer at the sediment-water interface along the whole line. This size of the high resistivity plume intensifies at low tide, indicating that more SGD occurs at low tide, which is in accordance with observations of tidally modulated discharge patterns via seepage meters and geochemical tracers [*Dulaiova et al.*, 2006]. Similar to the ER results in Kiholo Bay, the statistical evaluations (RMS and L2 norm values) of the ER data

distributions in Wailupe Beach Park guarantee high confidence level of the obtained results. However, we found that an overlying seawater column highly effects the resistivity measurements. Similar effect on the field collected data was also observed by *Swarzenski et al.* [2007] in a shoreline perpendicular array collected at Hood Canal, WA, during a full tide cycle when the cable was partially under water for the period of high tide. These effects are due to the fact that seawater has a much higher conductivity and this deforms the electrical field of the transmitted signal. In addition because seawater has much higher electrical conductivity rather than the underlying seafloor sediments, the electrical signal would preferentially flow through the water than through the sediment. As a result the signal received by the instrument is highly weakened. Although these are only speculations at this point, further detailed experiments need to be done in order to be able to perform reliable ER measurements in such tidally affected environments.

[21] The resistivity-based SGD rates presented in this work are in the range of other tracer estimates. This is an indication that both the ER evaluations and the assumptions made in our salinity mixing model are adequate and can be applied in similar coastal environments elsewhere. Site-specific results show that the total freshwater flux in Kiholo Bay, Big Island was about 40% larger than in Maunalua Bay, Oahu. Our estimates of fresh groundwater discharge in Maunalua Bay, based on a 12-h resistivity time series in Wailupe State Beach, was evaluated at about 2,950 m^3/d per single tide cycle, or in the case of two tides per day, this is ~5,900 m^3/d. A conservative estimate will result in 12 to 20% of the fresh water component in the SGD fluxes in Wailupe Beach Park. Lower values in resistivity of the formation water in Wailupe Beach (1 to 11 Ohm-m) also suggest a larger seawater component compared to Kiholo Bay for example (3–35 Ohm-m). This may be a plausible finding as *Oki et al.* [1999a] reported much lower water table levels in Oahu compared to the Big Island. A lower water table would create conditions for larger scale seawater intrusion into the aquifer; at these conditions, more seawater will be potentially exchanged during a tide cycle.

6. Conclusion

[22] We demonstrated that multichannel electrical resistivity can be used successfully to study fresh water–seawater interactions in volcanic coastal aquifers. Using ER images we were able to identify, compare, and contrast hydrogelogical subsurface features related to site-specific driving forces of SGD in two volcanic coastal areas in Hawaii, the Kona coast on the Big Island and Maunalua Bay on Oahu. Our images confirmed previous hypotheses that the SGD seepage in both areas is primarily from point (distinct) sources. However, while at Kiholo Bay the fresh water discharge is conveyed into lava tubes and lava flows formations, our images showed that the SGD at Wailupe Bay is expressed as submarine springs.

[23] A new model based on temporal changes of subsurface salinity distributions and measured resistivity and formation factors under different tide stages was developed to assess freshwater fluxes over a tidal cycle. We hypothesize that the same model could be used in reverse to calculate rates of seawater intrusion into aquifers. Such an application of the electrical resistivity method would have big potential in evaluating status of aquifer capacities and fresh water availability in the prospective of sea level rise and increasing groundwater pumping rates. To estimate this, one would have to measure ER subsurface distributions during rising tide. High resolution electrical resistivity images presented in this work proved that this geophysical tool can provide a more detailed blueprint of SGD flow patterns across the land-sea margin. In this study we coupled this information with findings about formation factors to calculate seepage rates using a simple salinity mixing model. However, as the images reflect clear defined areas of freshwater-saltwater interface, researchers who use tracer approaches could employ these images to constrain assumptions related to SGD source spatial distribution. Knowledge about the actual spatial distribution of subsurface changes could also be very useful for those who are interested in geochemical transformations in the subterranean estuary as freshwater-seawater interface is located at the steepest chemical gradients [*Charette et al.*, 2005].

[24] **Acknowledgments.** The authors would like to thank Joseph Kennedy, Christine Waters, and Kayla Holleman, students from the Department of Geology and Geophysics, University of Hawai'i at Mānoa, who helped during the field work. The students and part of this research were supported by NSF's IMUA III EPSCoR program. Special thanks to John Bratton and Nancy Prouty for informal reviews and discussions before submission. We also would like to acknowledge Rob Evans and one anonymous reviewer who contributed with their comments in improving the scientific content and quality of this manuscript. Peter W. Swarzenski thanks the USGS Coastal and Marine Geology Program for support. The use of trade names is for descriptive purposes only and does not imply endorsement by the U.S. Government.

References

Advanced Geosciences, Inc. (2009), Instruction Manual for EarthImager 2D, Version 2.4.0, Resistivity and IP Inversion Software, Austin, Tex. [Available at http://www.agiusa.com.]

Archie, G. E. (1942), The electrical resistivity logs as an aid in determining some reservoir characteristics, *Trans. AIME*, *146*, 54–62.

Baker, R. D., and P. F. Worthington (1973), The hydrological and electrical anisotropy of the Bunter sandstone of northwest Lancashire, *Q. J. Eng. Geol.*, *6*, 169–175, doi:10.1144/GSL.QJEG.1973.006.02.04.

Bratton, J. (2010), The three scales of submarine groundwater flow and discharge across passive continental margins, *J. Geol.*, *118*, 565–575, doi:10.1086/655114.

Cable, J. E., W. C. Burnett, J. P. Chanton, and G. L. Weatherly (1996), Estimating groundwater discharge into the northeastern Gulf of Mexico using radon-222, *Earth Planet. Sci. Lett.*, *143*, 591–604, doi:10.1016/S0012-821X(96)00173-2.

Charette, M. A., E. R. Sholkovitz, and C. M. Hansel (2005), Trace element cycling in a subterranean estuary: Part I. Geochemistry of the permeable sediments, *Geochim. Cosmochim. Acta*, *69*, 2095–2109, doi:10.1016/j.gca.2004.10.024.

Charette, M. A., W. S. Moore, and W. C. Burnett (2008), Uranium- and thorium-series nuclides as tracers of submarine groundwater discharge, in *U-Th Series Nuclides in Aquatic Systems*, vol. 13, *Radioactivity in the Environment*, edited by S. Krishnaswami and J. K. Cochran, pp. 155–191, Elsevier, New York.

Constable, S. C., R. L. Parker, and C. G. Constable (1987), Occam's inversion: A practical algorithm for generating smooth models from electromagnetic sounding data, *Geophysics*, *52*, 289–300, doi:10.1190/1.1442303.

Dimova, N. T., W. C. Burnett, and K. Speer (2011), A natural tracer investigation of the hydrological regime of Spring Creek Springs, the largest submarine spring system in Florida, *Cont. Shelf Res.*, *31*, 731–738, doi:10.1016/j.csr.2011.01.010.

Dulaiova, H., W. C. Burnett, J. P. Chanton, W. S. Moore, H. J. Bokuniewicz, M. A. Charette, and E. Sholkovitz (2006), Assessment of submarine groundwater discharges into West Neck Bay, New York, via natural tracers, *Cont. Shelf Res.*, *26*(16), 1971–1983, doi:10.1016/j.csr.2006.07.011.

Ernstson, K., and R. Kirsh (2006), Geoelectrical Methods, in *Groundwater Geophysics: A Tool for Hydrogeology*, edited by R. Kirsch, pp. 84–117, Springer, New York.

Evans, R. L., and D. Lizarralde (2003), Geophysical evidence for karst formation associated with offshore groundwater transport: An example from North Carolina, *Geochem. Geophys. Geosyst.*, *4*(8), 1069, doi:10.1029/2003GC000510.

Evans, R. L., and D. Lizarralde (2011), The competing impacts of geology and groundwater on electrical resistivity around Wrightsville Beach, NC, *Cont. Shelf Res.*, *3*, 841–848, doi:10.1016/j.csr.2011.02.008.

Fofonoff, N. P., and R. C. Millard Jr. (1983), Algorithms for computation of fundamental properties of seawater, *UNESCO Tech. Pap. Mar. Sci.*, *44*.

Gingerich, S. B., and C. I. Voss (2005), Three-dimensional variable-density flow simulation of a coastal aquifer in southern Oahu, USA, *Hydrogeol. J.*, *13*, 436–450, doi:10.1007/s10040-004-0371-z.

Hoefel, F. G., and R. L. Evans (2001), Impact of low salinity porewater on seafloor electromagnetic data: A means of detecting submarine groundwater discharge?, *Estuarine Coastal Shelf Sci.*, *52*, 179–189, doi:10.1006/ecss.2000.0718.

Holleman, K. (2011), Comparison of submarine groundwater-derived nutrients from leeward flanks of the islands of Oahu and Hawaii, MS thesis, Dep. of Geol. and Geophys., Univ. of Hawai'i at Mānoa, Honolulu.

Jackson, P. D., K. B. Briggs, R. C. Flint, R. J. Holyer, and J. C. Sandidge (2002), Two- and three-dimensional heterogeneity in carbonate sediments using resistivity imaging, *Mar. Geol.*, *182*, 55–76, doi:10.1016/S0025-3227(01)00228-6.

Johnson, A. G., C. R. Glenn, W. C. Burnett, R. N. Peterson, and P. G. Lucey (2008), Aerial infrared imaging reveals large nutrient-rich groundwater inputs to the ocean, *Geophys. Res. Lett.*, *35*, L15606, doi:10.1029/2008GL034574.

Keller, G. V., and F. C. Frischknecht (1966), *Electrical Methods in Geophysical Prospecting*, Pergamon, Oxford, U. K.

Khalil, A. M., and F. A. Monterio Santos (2009), Influence of degree of saturation in the electrical resistivity-hydraulic conductivity relationship, *Surv. Geophys.*, *30*, 601–615, doi:10.1007/s10712-009-9072-4.

Knee, K. L., J. H. Street, E. E. Grossman, A. B. Boehm, and A. Paytan (2010), Nutrient inputs to the coastal ocean from submarine groundwater discharge in a groundwater-dominated system: Relation to land use (Kona coast, Hawaii, U.S.A.), *Limnol. Oceanogr.*, *55*(3), 1105–1122, doi:10.4319/lo.2010.55.3.1105.

Langenheim, V. A. M., and D. A. Clague (1987), The Hawaiian-Emperior volcanic chain, part II, Stratigraphic framework of volcanic rocks of the Hawaiian Islands, in *Volcanism in Hawaii*, edited by R. W. Decker, T. L. Wright, and P. H. Stauffer, *U.S. Geol. Surv. Prof. Pap.*, *1350*, 55–84.

Loke, M. H. (2011), Tutorial: 2-D and 3-D electrical imaging surveys, Geotomo Software Sdn. Bhd., Penang, Malaysia. [Available at http://www.geoelectrical.com.]

Macdonald, G. A., A. T. Abbott, and F. L. Peterson (1983), *Volcanoes in the Sea: The Geology of Hawaii*, 2nd ed., Univ. of Hawaii Press, Honolulu.

Manheim, F. T., D. E. Krantz, and J. F. Bratton (2004), Studying ground water under Delmarva coastal bays using electrical resistivity, *Ground Water*, *42*(7), 1052–1068, doi:10.1111/j.1745-6584.2004.tb02643.x.

McGowan, M. (2004), Submarine groundwater discharge: Freshwater and nutrient input into Hawaii's coastal zone, MS thesis, Dep. of Geol. and Geophys., Univ. of Hawai'i at Mānoa, Honolulu.

Michael, H. A., A. E. Mulligan, and C. F. Harvey (2005), Seasonal oscillations in water exchange between aquifers and the coastal ocean, *Nature*, *436*, 1145–1148, doi:10.1038/nature03935.

Mulligan, A. E., R. L. Evans, and D. Lizarralde (2007), The role of paleochannels in groundwater/seawater exchange, *J. Hydrol.*, *335*, 313–329, doi:10.1016/j.jhydrol.2006.11.025.

Mullineaux, D. R., D. W. Peterson, and D. R. Crandell (1987), Volcanic hazards in the Hawaiian Islands., in *Volcanism in Hawaii*, edited by R. W. Decker, T. L. Wright, and P. H. Stauffer, *U.S. Geol. Surv. Prof. Pap.*, *1350*, 55–84.

Oki, D. S., G. W. Tribble, W. R. Souza, and E. L. Bolke (1999a), Groundwater sources in Kaloko-Honokohau National Historic Park, Island of Hawaii, and numerical simulation of the effect of ground-water withdraws, *U.S. Geol. Surv. Water Resour. Invest. Rep.*, *99-4070*.

Oki, D. S., S. B. Gingerich, and R. L. Whitehead (1999b), Ground water atlas of the United States: Alaska, Hawaii, Puerto Rico and the U. S. Virgin Islands, *HA 730-N*, U.S. Geol. Surv., Reston, Va.

Perkin, R., and E. Lewis (1980), The Practical Salinity Scale 1978: Fitting the data, *J. Oceanic Eng.*, *5*(1), 9–16, doi:10.1109/JOE.1980.1145441.

Peterson, R. N., W. C. Burnett, C. R. Glenn, and A. G. Johnson (2009), Quantification of point-source groundwater discharges to the ocean from the shoreline of the Big Island, Hawaii, *Limnol. Oceanogr.*, *57*(3), 890–904, doi:10.4319/lo.2009.54.3.0890.

Reilly, T. E., and A. S. Goodman (1985), Quantitative analysis of saltwater-freshwater relationships in groundwater systems-a historical perspective, *J. Hydrol.*, *80*, 125–160, doi:10.1016/0022-1694(85)90078-2.

Ruppel, C., G. Schultz, and S. Kruse (2000), Anomalous fresh water lens morphology on a strip barrier island, *Ground Water*, *38*(6), 872–881, doi:10.1111/j.1745-6584.2000.tb00686.x.

Samouelian, A., I. Cousin, A. Tabbagh, A. Bruand, and G. Richard (2005), Electrical resistivity survey in soil science: A review, *Soil Tillage Res.*, *83*, 173–193, doi:10.1016/j.still.2004.10.004.

Schultz, G., and C. Ruppel (2005), Inversion of inductive electromagnetic data in highly conductive terrains, *Geophysics*, *70*(1), 16–28, doi:10.1190/1.1852775.

Shade, P. J., and W. D. Nichols (1996), Water budget and effect of land-use changes on ground-water recharge, Oahu, Hawaii, *U.S. Geol. Surv. Prof. Pap.*, *1412-C*.

Soupios, P. M., M. Kouli, F. Vallianatos, A. Vafidis, and G. Stavroulakis (2007), Estimation of aquifer hydraulic parameters from surficial geophysical methods: A case study of Keritis Basin in Chania (Crete-Greece), *J. Hydrol.*, *338*, 122–131, doi:10.1016/j.jhydrol.2007.02.028.

Stearns, H. T. (1940), Supplement to the geology and ground-water resources of the island of Oahu, Hawaii, *Hawaii Div. Hydrogr., Bull. 5*.

Street, H. J., K. L. Knee, E. E. Grossman, and A. Paytan (2008), Submarine groundwater discharge and nutrient addition to the coastal zone and coral reefs of leeward Hawai'i, *Mar. Chem.*, *109*, 355–376, doi:10.1016/j.marchem.2007.08.009.

Swartz, J. H. (1937), Resistivity-studies of some salt-water boundaries in the Hawaiian Islands, *Eos Trans. AGU*, *18*, 387–393.

Swarzenski, P. W., W. C. Burnett, W. J. Greenwood, B. Herut, R. Peterson, N. Dimova, Y. Shalem, Y. Yechieli, and Y. Weinstein (2006), Combined time-series resistivity and geochemical tracer techniques to examine submarine groundwater discharge at Dor Beach, Israel, *Geophys. Res. Lett.*, *33*, L24405, doi:10.1029/2006GL028282.

Swarzenski, P. W., F. W. Simonds, A. J. Paulson, S. Kruse, and C. Reich (2007), A geochemical and geophysical examination of submarine groundwater discharge and associated nutrient loading estimates into Lynch Cove, Hood Canal, WA, *Environ. Sci. Technol.*, *41*, 7022–7029, doi:10.1021/es070881a.

Swarzenski, P. W., J. A. Izbicki, E. E. Grossman, C. R. Glenn, C. A. Plath, and J. L. Kelly (2009), A multiproxy tracer approach to submarine groundwater discharge studies: Examples from Santa Barbara, CA and Maunalua Bay, Oah'u, HI, *Geochim. Cosmochim. Acta*, *73*, A1299.

Taniguchi, M., W. C. Burnett, C. Smith, R. J. Pausen, D. O'Rourke, S. L. Krupa, and J. Christoff (2003), Spatial and temporal distributions of submarine groundwater discharge rates obtained from various types of seepage meters at a site in the Northeastern Gulf of Mexico, *Biogeochemistry*, *66*, 35–53, doi:10.1023/B:BIOG.0000006090.25949.8d.

Urish, D. W., and T. E. McKenna (2004), Tidal effects on ground water discharge through a sandy marine beach, *Ground Water*, *42*(7), 971–982, doi:10.1111/j.1745-6584.2004.tb02636.x.

Viso, R., C. McCoy, P. Gayes, and D. Quafisi (2010), Geological controls on submarine groundwater discharge in Long Bay, South Carolina (USA), *Cont. Shelf Res.*, *30*, 335–341, doi:10.1016/j.csr.2009.11.014.

Waxman, M. H., and L. J. M. Stairs (1968), Electrical conductivities in oil-bearing shally sands, *SPEJ Soc. Pet. Eng. J.*, *8*, 107–122, doi:10.2118/1863-A.

Winsauer, W. O., H. M. Shearin, P. H. Masson, and M. Williams (1952), Resistivity of brine-saturated sands in relation to pore-geometry, *Bull. AAPG*, *36*, 253–277.

Worthington, P. F. (1972), The use of resistivity logging to estimate borehole yield from a matrix-conducting sandstone, *Q. J. Eng. Geol.*, *4*, 263–279, doi:10.1144/GSL.QJEG.1971.004.04.01.

Worthington, P. F. (1993), The uses and abuses of the Archie equations, 1: The formation factor-porosity relationship, *J. Appl. Geophys.*, *30*, 215–232, doi:10.1016/0926-9851(93)90028-W.

Zohdy, A. A. R. (1968), The effect of current leakage and electrode spacing errors on resistivity measurements, in *Geological Survey Research 1968*, *U.S. Geol. Surv. Prof. Pap.*, *600-D*, 264–268.

Zohdy, A. A. R., and D. B. Jackson (1969), Application of deep electrical soundings for groundwater exploration in Hawaii, *Geophysics*, *34*(4), 584–600, doi:10.1190/1.1440033.

Zohdy, A. A. R., G. P. Eaton, and D. R. Mabey (1974), Application of surface geophysics to ground-water investigations, *U.S. Geol. Surv. Tech. Water Resour. Invest.*, *Book 2*, *Chap. D1*.

N. T. Dimova, Institute of Marine Sciences, University of California, Santa Cruz, CA 95060, USA. (natodi@gmail.com)

H. Dulaiova and C. R. Glenn, Department of Geology and Geophysics, University of Hawai'i at Mānoa, Honolulu, HI 96822, USA.

P. W. Swarzenski, U.S. Geological Survey, Santa Cruz, CA 95060, USA.